sustainability

MDPI

Article

Spatiotemporal Dynamics, Drivers, and Landscape Ecological Risk of Coastal Wetlands in the Yellow River Delta: A Pattern–Driver–Risk Framework with GWR

Peiyue Zhu [1,†], Yitong Yin [1,†], Rongjin Yang [2], Guoying Dong [1], Zechen Song [3], Ting Zhou [1], Le Zhang [2], Meiying Sun [2] and Xiuhong Li [1,4,*]

[1] State Key Laboratory of Remote Sensing and Digital Earth, Faculty of Geographical Science, Beijing Normal University, Beijing 100875, China; 202321051238@mail.bnu.edu.cn (P.Z.); yyt0910@outlook.com (Y.Y.); 11112011086@bnu.edu.cn (G.D.); 202321051263@mail.bnu.edu.cn (T.Z.)
[2] State Key Laboratory of Environmental Criteria and Risk Assessment, Chinese Research Academy of Environmental Sciences, No. 8, Da Yang Fang, An Wai, Chao Yang District, Beijing 100012, China; yrj_craes@outlook.com (R.Y.); zhangle@craes.org.cn (L.Z.); sun.meiying@craes.org.cn (M.S.)
[3] School for Environment and Sustainability, University of Michigan, Ann Arbor, MI 48109, USA; szechen@umich.edu
[4] Beijing Engineering Research Center for Global Land Remote Sensing Products, Faculty of Geographical Science, Beijing Normal University, Beijing 100875, China
* Correspondence: lixh@bnu.edu.cn; Tel.: +86-13621166693
† These authors contributed equally to this work.

Abstract

Coastal wetlands, as sensitive ecological interfaces of land–sea interactions, provide regulating functions and ecosystem service values for maintaining regional ecological security. To achieve systematic restoration of ecological functions and intelligent management of resources in coastal wetlands, it is critical to deconstruct the evolution patterns of their landscape configurations across multiple spatiotemporal scales and precisely identify driving factors and ecological risk transmission mechanisms. This study constructs a trinity framework of "pattern evolution-driver analysis-risk assessment" for landscape ecological risk (LER) evaluation, integrating spatial statistical analyses (Standard Deviational Ellipse, Land Use Transition Matrix) and Geographically Weighted Regression (GWR) models to systematically analyze the spatiotemporal evolution characteristics and multidimensional driving mechanisms of landscape patterns in the Yellow River Delta (YRD), a typical coastal wetland, from 2000 to 2023. The results are as follows: (1) total wetland area initially declines followed by partial recovery, with natural wetlands decreasing persistently and artificial wetlands expanding; (2) Gross domestic product (GDP) and temperature (TMP) are identified as the primary drivers of wetland evolution; (3) Wetland LER levels significantly increase from 2015 to 2020, with the proportion of high-risk areas rising from 10% in 2015 to 23% in 2020; (4) LER is predominantly characterized by High-High (H-H) clustering, with Moran's I values ranging from 0.493 to 0.672 (all $p < 0.001$), indicating significant positive spatial autocorrelation. The wetland LER assessment framework developed in this study, grounded in a land–sea integrated perspective, provides decision-making support and theoretical foundations for formulating differentiated wetland restoration strategies and optimizing coastal ecological security patterns.

Keywords: wetland; spatiotemporal evolution; drivers of evolution; landscape ecological risk; Geographically Weighted Regression; wetland sustainability

Check for updates

Academic Editor: Ana Cláudia Teodoro

Received: 22 April 2026
Revised: 29 May 2026
Accepted: 4 June 2026
Published: 9 June 2026

Copyright: © 2026 by the authors. Licensee MDPI, Basel, Switzerland. This article is an open access article distributed under the terms and conditions of the Creative Commons Attribution (CC BY) license.

1. Introduction

As one of the most productive ecosystems on Earth, wetlands occupy <7% of global land area yet sustain 40% of biodiversity and deliver $47.4 trillion in annual ecosystem services [1,2], including carbon sequestration, storm buffering, and fisheries [3–5]. However, intensive anthropogenic activities have caused a 35% loss of natural coastal wetlands globally, with artificial wetland expansion outpacing natural recovery [6,7]. This "ecological substitution" (natural wetlands replaced by reservoirs, aquaculture ponds) triggers cascading risks: mangrove loss reduces coastal resilience, salt marsh degradation releases stored carbon, and artificial wetland homogenization exacerbates biotic homogenization [8]. The 1971 Ramsar Convention mandates wetland conservation [9]. In 2015, the UN included wetland protection in SDG 6.6 and SDG 14.2 [7,10,11].

China has enacted the Wetland Protection Law and the National Wetland Protection Plan (2022–2030). By 2020, China had 64 Ramsar Sites and thousands of protected areas [12,13].

From a theoretical perspective, landscape ecological risk (LER) is rooted in the principle that landscape patterns (e.g., fragmentation, separation, fractal dimension) can indicate ecological processes and the potential for adverse effects. This study conceptualizes the Yellow River Delta as a coupled human-environment system, where natural hydrological and climatic drivers interact with socioeconomic activities (agriculture, aquaculture, urbanization) through feedback loops. The concepts of resilience and vulnerability are central: vulnerability refers to the susceptibility of wetland ecosystems to damage from external disturbances, while resilience denotes their capacity to recover. According to ecosystem succession theory, early-successional wetlands have low biodiversity and weak resistance, making them more vulnerable. Integrating pattern evolution, driver identification, and risk assessment yields a complete causal chain from "what is happening" (pattern), "why it is happening" (drivers), to "what are the consequences" (risk), thereby providing a theoretical basis for adaptive management.

Climate change and human activities have altered wetland LULC, manifesting as mangrove/salt flat loss and reservoir/paddy expansion. These changes affect ecosystem and landscape dynamics, generating ecological risks [14]. Ecological risk assessment quantifies the negative impacts of environmental change and human activities, helping resolve conflicts between ecological protection and economic development [14,15].

Two main ecological risk models exist: the "source-sink" method (for clear pressure sources) and the landscape pattern method. For LULC-driven risks, the landscape pattern method is more appropriate because it considers both hazard and fragmentation impacts [14]. This study adopts landscape ecological risk (LER) assessment, integrating disturbance and vulnerability indices for spatially explicit mapping.

Extensive research has quantified LER [16,17]. Road network expansion increases LER [18,19] by amplifying habitat fragmentation [20]. Lake studies show that unsustainable water management reduces lake area and increases LER [21–24]. LER has also been assessed in hilly mountainous and urbanized areas [25–27].

However, these studies have not addressed coupled pattern–driver–risk dynamics in a large, rapidly changing coastal delta. This gap motivates our case study of the Yellow River Delta (YRD). Two gaps remain: (1) LER assessments have focused on fragile zones (lakes, hills, roads, cities) but have underexplored coastal wetland reserves and avian breeding grounds. (2) Most studies lack systematic integration of pattern evolution, driver identification, and risk assessment. Some attempts exist (e.g., Zeng et al. [25] in a mountainous area), but they did not capture spatial non-stationarity or were set in non-coastal environments. Our contribution is (i) applying spatially explicit GWR to reveal geographically varying driver effects in a coastal delta, and (ii) coupling GWR results directly with LER clustering for zone-based management.

Coastal wetlands face dual natural and human pressures, leading to uneven risk patterns. Without a framework integrating risk dynamics, drivers, and aggregation, conservation policies may have a limited effect.

The theoretical implications of integrating pattern evolution, driver analysis, and risk assessment are threefold. First, pattern evolution reveals the direction and intensity of landscape change under combined natural and human pressures. Second, driver analysis using GWR captures spatial non-stationarity, acknowledging that the same driver may have opposing effects in different locations. Third, risk assessment translates these spatial associations into management-relevant outcomes. Together, they form a diagnostic framework that moves beyond description to attribution and action, which is essential for coupled human-environment systems such as coastal deltas.

The YRD is a key stopover site in the East Asian-Australasian Flyway and a national-level nature reserve preserving the world's youngest, largest, and most complete estuarine wetland ecosystem [28,29]. Yet it is ecologically fragile and highly sensitive. Rapid population and socioeconomic growth have led to construction land, aquaculture ponds, and farmland replacing original wetlands, increasing fragmentation and LER [15,30]. Over 10 ecological restoration projects have also altered land use, further affecting LER [30]. Thus, investigating YRD wetland dynamics and establishing a robust LER model is imperative.

To address the gaps, we propose a tripartite framework of "pattern evolution–driving mechanisms–risk assessment". Objectives: (1) quantify spatiotemporal wetland type transitions (2000–2023); (2) develop a GWR model to elucidate spatially non-stationary driving mechanisms; (3) construct an LER model at the risk-unit scale and interpret clustering via spatial autocorrelation. Previous coastal LER assessments used global regression models assuming uniform effects; our method reveals how key drivers vary geographically. Our contributions: (i) extend LER assessment to a critical but under-examined coastal wetland reserve; (ii) move from global averages to spatially explicit, locally adaptive risk diagnosis; (iii) demonstrate how pattern–driver–risk coupling informs differentiated restoration strategies.

2. Materials and Methods

2.1. Overview of the Study Area

The YRD (Figure 1) is located in the northeastern part of Shandong Province (37°20′–38°10′, 118°10′–119°30′), with an annual average temperature (TMP) ranging from 12.1 °C to 13.1 °C and annual average precipitation (PRE) between 530 mm and 630 mm [31,32]. The total study area is approximately 5934 km^2, covering parts of both Dongying City and Binzhou City. Situated at the intersection of marine, riverine, and terrestrial ecosystems, its unique geographical location has created an area with high productivity and rich biodiversity. It is a region of integrated agricultural, fishing, and petrochemical development, making it not only significant in global wetland ecosystem research but also owing to its substantial economic value. Given that the core area of the YRD is situated within Dongying City, the statistical data from Dongying City are adopted as a representative proxy for the entire YRD. In 2023, Dongying City achieved a gross domestic product (GDP) of 389.906 billion yuan, with the total output value of agriculture, forestry, animal husbandry, and fishery reaching 38.606 billion yuan.

However, owing to the combined effects of global warming and intensified human activities, YRD wetlands have experienced significant degradation [31,32]. For example, under the impact of rising sea levels caused by global warming and extreme climate events such as heavy rainfall and storm surges, the coastlines of YRD wetlands have eroded, and natural wetlands such as tidal flats have been damaged. Human activities such as agricultural reclamation, aquaculture, oil extraction, and dam construction have occupied

large areas of natural wetlands [33,34]. These changes in land use/land cover (LULC) types and their spatiotemporal patterns, caused by either natural or human factors, directly or indirectly affect the changes in ecosystems and landscape patterns, further exacerbating the ecological risks to YRD wetlands.

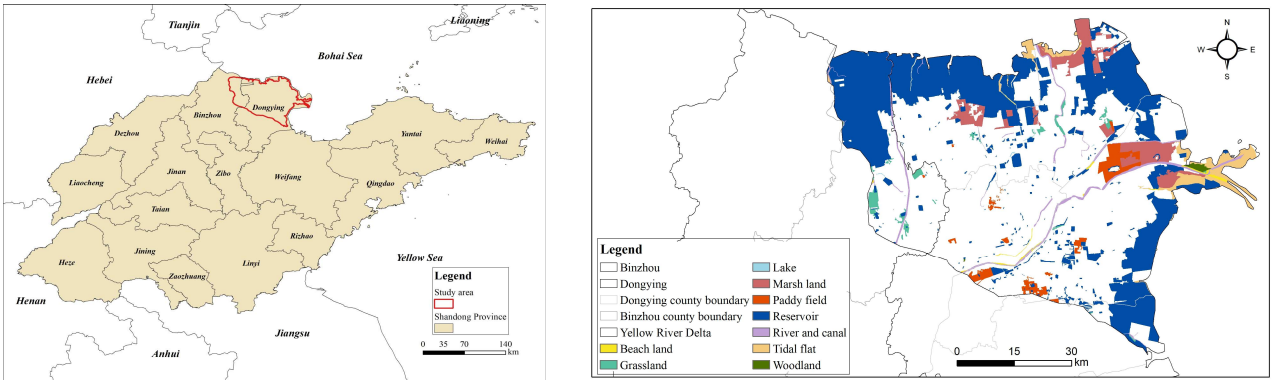


Figure 1. Location of the study area.

2.2. Data Sources

In this study, LULC data for the years 2000, 2005, 2010, 2015, 2020, and 2023 were acquired from the Resource and Environmental Science Data Center of the Chinese Academy of Sciences (https://www.resdc.cn/). Through field investigations and literature reviews, the original LULC datasets were reclassified into nine wetland categories: paddy field, woodland, grassland, river and canal, lake, reservoir, tidal flat, beach land and marsh land. This classification follows the Chinese national wetland classification standard (GB/T 24708-2009 [35]) issued by the Standardization Administration of China. Under this standard, forested and meadow areas with specific hydrological conditions can be defined as natural wetlands. In the Yellow River Delta, the "woodland" and "grassland" categories correspond to natural willow wetlands, shrub wetlands, and meadow wetlands that are periodically inundated or waterlogged, as documented by the regional wetland information system and previous studies (see justification in Section 2.3.4). Thus, while the Ramsar definition (cited in the Introduction) emphasizes "water saturation" as a key criterion, the operational classification used here is consistent with the national standard and the local ecological reality. The TMP, PRE and digital elevation model (DEM) data were obtained from the Resource and Environment Science Data Platform (https://www.resdc.cn/). The fractional vegetation cover (FVC) dataset was obtained from the National Scientific Data Center for the Tibetan Plateau (https://data.tpdc.ac.cn/). The POP data were obtained from the LandScan Global Population Dataset (https://landscan.ornl.gov/). Road network data were obtained from the OpenStreetMap platform (https://www.openstreetmap.org/). The evapotranspiration (ET) data were obtained from the MOD16 ET datasets (http://www.ntsg.umt.edu/project/mod16, accessed on 1 April 2026). The GDP data were obtained from the Nature Scientific data website [36].

During the data processing phase, all raster images were projected to the Albers Projection using ArcGIS, and the geographic coordinate system was standardized to GCS_WGS_1984. The original spatial resolutions of the input datasets are as follows: LULC (30 m), TMP (1 km), PRE (1 km), DEM (500 m), FVC (1 km), POP (1 km), ET (500 m), and GDP (1 km). To unify all datasets to a consistent spatial resolution, we resampled all coarser-resolution grids to a 30 m × 30 m cell size using the nearest neighbor resampling method. This method was chosen because it preserves the original category values for discrete variables (e.g., LULC types) and avoids introducing artificial values through interpolation. However, we acknowledge that nearest neighbor resampling does not add

new information and may result in a patchy, step-like appearance for continuous variables (e.g., TMP, PRE, ET, GDP, POP). Moreover, aggregating ~1 km population and temperature data to a 30 m grid does not create genuine fine-scale heterogeneity; instead, each 30 m cell within a coarse pixel receives the same value. This limitation may smooth out local variability and affect the precision of GWR coefficient estimates in heterogeneous areas. Despite these constraints, the consistent use of nearest neighbor resampling ensures that no artificial spatial patterns are introduced, and the overall spatial trends at the landscape scale remain interpretable.

2.3. Methods

2.3.1. Research Framework

First, utilizing the 2000–2023 LULC datasets, a land dynamic transfer matrix was constructed to quantify the spatiotemporal conversion patterns of wetland types in the YRD. Concurrently, the standard deviational ellipse (SDE) method was employed to characterize directional shifts in wetland spatial distribution. This dual analytical approach established a foundational framework for interpreting wetland evolution dynamics. Second, building upon the identified spatiotemporal evolution patterns, eight driving factors were integrated. The Ordinary Least Squares (OLS) model and GWR model were synergistically applied to reveal spatially heterogeneous driving mechanisms, thereby constructing a progressive analytical framework for disentangling natural and anthropogenic influences. Third, leveraging insights from preceding stages, a LER assessment model was developed by synthesizing landscape disturbance and vulnerability indices. Spatial overlay analysis and geovisualization techniques were implemented to quantitatively map the spatiotemporal differentiation of LER across the study area from 2000 to 2023. This methodological advancement elevated the analytical dimension from pattern characterization to risk evaluation. Finally, grounded in LER assessment outcomes, global spatial autocorrelation analysis using Moran's Index was conducted to identify risk aggregation patterns. Hotspot and coldspot detection further delineated spatial association characteristics of LER. Collectively, these analyses formed an integrated research framework encompassing "pattern evolution-driver analysis-risk assessment", achieving a closed-loop scientific inquiry into wetland ecosystem dynamics.

2.3.2. Analysis of the Standard Deviational Ellipse and Centroid

For *SDE*, compared with traditional centroid shift analysis or simple area statistics, *SDE* simultaneously captures the spatial orientation, dispersion, and expansion trends of wetland patches by providing geometric attributes such as azimuth angle, major axis, minor axis, and flattening. This enables a visual and quantitative characterization of wetland expansion or contraction along different directions during 2000–2023, and can be used to analyze the dynamic spatial patterns between natural and artificial wetlands in land–sea interaction zones. As a statistical method in geographic information systems, *SDE* is used to study spatial relationships among geographic elements, and the long and short axes of its ellipses can reflect the spatial distribution direction and degree of deviation of geographic features [37]. In this study, the *SDE* was utilized to study the overall distribution and change characteristics of YRD wetlands. The steps of the *SDE* calculation are as follows, following the standard formulation [38,39]:

First, calculate the center of the *SDE*:

$$SDE_x = \sqrt{\frac{\sum_{i=1}^{n} \left(x_i - \overline{X}\right)^2}{n}} \quad (1)$$

$$SDE_y = \sqrt{\frac{\sum_{i=1}^{n}(y_i - \overline{Y})^2}{n}} \quad (2)$$

Second, the azimuth angle is calculated:

$$\tan\theta = \frac{\left(\sum_{i=1}^{n}\tilde{x}_i^2 - \sum_{i=1}^{n}\tilde{y}_i^2\right) + \sqrt{\left(\sum_{i=1}^{n}\tilde{x}_i^2 - \sum_{i=1}^{n}\tilde{y}_i^2\right)^2 + 4\left(\sum_{i=1}^{n}\tilde{x}_i\tilde{y}_i\right)^2}}{2\sum_{i=1}^{n}\tilde{x}_i\tilde{y}_i} \quad (3)$$

Third, the standard deviation distance is calculated:

$$\sigma_x = \sqrt{\frac{\sum_{i=1}^{n}\left(\tilde{x}_i\cos\theta - \tilde{y}_i\sin\theta\right)^2}{n}} \quad (4)$$

$$\sigma_y = \sqrt{\frac{\sum_{i=1}^{n}\left(\tilde{x}_i\sin\theta - \tilde{y}_i\cos\theta\right)^2}{n}} \quad (5)$$

where n represents the number of wetland types in the YRD; (x_i, y_i) represents the spatial coordinates of different types of wetlands; $(\overline{X}, \overline{Y})$ represents the arithmetic mean center of the centers of all the types of wetlands; θ represents the azimuth angle of the ellipse; $\tilde{x}_i$ and $\tilde{y}_i$ represent the differences in the centers of the different types of wetlands with the mean center; and σ_x and σ_y represent the standard deviations along the X and Y axes, respectively.

2.3.3. Analysis of the Driving Factors of Wetland Evolution

OLS is a common method used to analyze the relationship between two or more variables, and is calculated as follows [40]:

$$y = \beta_0 + \sum_{k=1}^{p}\beta_k x_k + \varepsilon \quad (6)$$

OLS assumes that the parameters and coefficients of the statistical model are constant across regions [41,42]. However, the Yellow River Delta, as a land–sea ecotone, exhibits strong spatial heterogeneity in both natural conditions and anthropogenic activities. The influence of these drivers on landscape ecological risk (LER) is likely to vary with geographic location, distance from the coastline, and land use intensity. Therefore, the failure to consider spatial correlation and non-stationarity is a major weakness of OLS in spatial modeling.

To address this issue, Geographically Weighted Regression (GWR) is employed. GWR explicitly captures spatial non-stationarity by fitting local regressions, where different weights are assigned to different points in the study area. The weights decrease with increasing distance between the observation point and the reference point, following Tobler's first law of geography [43]. This approach reveals spatially varying contributions of each driver, making GWR more suitable than OLS or spatial lag models for guiding differentiated, zone-based wetland management strategies. It should be noted that, due to the limited availability of long-term time-series data, this study considers only eight driving factors (PRE, TMP, ET, FVC, DEM, GDP, POP, and distance to roads/railways). For a coastal delta system such as the Yellow River Delta, other factors—including relative sea-level rise, water salinity, sediment load and discharge from the Reservoir, ecological water replenishment volumes, and aquaculture intensity—may also play important roles in wetland evolution. Owing to the difficulty of obtaining complete datasets for these variables over the study period (2000–2023), they are not included in the present analysis.

The GWR model can calculate the estimated coefficients at any point in the study area [41]. It is calculated as follows:

$$y_i = \beta_0(\mu_i, v_i) + \sum_k \beta_k(\mu_i, v_i)X_{ik} + \varepsilon_i \quad (7)$$

where y_i is the dependent variable; X_{ik} is the explanatory variable; (μ_i, v_i) denotes the spatial location; β_0 is the regression constant term; β_k is the local estimated coefficient of the independent variable; and ε_i denotes the random error term.

In this study, we used the bisquare function to determine the spatial weights and the AICc (corrected Akaike Information Criterion) method to select the optimal bandwidth. The AICc is preferred over AIC in GWR because it provides a better trade-off between model fit and complexity, especially for small sample sizes. We adopted an adaptive bandwidth (specified in terms of the number of nearest neighbours) to accommodate the varying spatial density of the risk evaluation units. The optimal bandwidth was determined by minimizing the AICc value across a range of candidate neighbour counts.

2.3.4. Assessment of Wetland Ecological Risks

The study area was divided into a 900 m × 900 m grid, resulting in a total of 665 risk evaluation units. The grid size was selected to be 2–5 times the average patch area in the study area, following the standard criterion in landscape ecological risk assessment to preserve patch integrity and avoid excessive fragmentation or over-smoothing of spatial heterogeneity [25]. The average patch area of wetlands in the YRD across all years is approximately 0.3–0.5 km^2 (calculated from the LULC data), so the 900 m × 900 m (0.81 km^2) grid falls within the recommended 2–5 times range. The steps for calculating the LER index for each unit are as follows [25]:

First, the wetland landscape disturbance index is calculated:

$$C_i = \frac{n_i}{A_i} \quad (8)$$

where n_i is the number of patches of wetland type i; A_i is the area of wetland type I; C_i is the landscape fragmentation index.

$$N_i = \frac{1}{2} \times \sqrt{\frac{n_i}{A_i}} \times \frac{A}{A_i} \quad (9)$$

N_i is the landscape separation index; A is the total area of all wetlands.

$$F_i = 2\ln(L_i/4)/\ln A_i \quad (10)$$

F_i is the landscape fractional dimension index of wetland type $\boldsymbol{i}$; $\boldsymbol{L_i}$ is the perimeter of wetland type $\boldsymbol{i}$.

$$E_i = aC_i + bN_i + cF_i \quad (11)$$

where a, b, and $\boldsymbol{c}$ are the weights of each index, $a + b + c = 1$. In accordance with related studies [25] and considering the characteristics of the study area, we assigned weights of 0.5, 0.3 and 0.2, respectively.

Second, the wetland landscape vulnerability index is calculated. In the early stage of ecosystem succession, the food chain structure is simple, biodiversity is low, and the ability to resist external disturbances is weak [25,44]. Therefore, on the basis of a comprehensive consideration of the landscape characteristics of the study area and the results of previous studies [45], this study refers to the wetland classification system widely adopted in studies on the dynamics of the Yellow River Delta wetlands and assigns values to

nine wetland types as follows [46,47]. The specific vulnerability ranking is justified as follows: marsh lands are mostly distributed in low-lying, water-logged areas with simple vegetation and high environmental fluctuations, making them extremely sensitive to external disturbances—thus assigned the highest vulnerability of 9. Beach lands and tidal flats are located in the land–sea ecotone, directly affected by tides and storm surges, with limited ecological buffering capacity—assigned 8 and 7, respectively. Artificial wetlands (reservoirs and paddy fields), although structurally simple, are subject to human management (e.g., water regulation, fertilization) and therefore have a certain capacity to resist disturbances—assigned 6 and 3, respectively (with reservoirs having a simpler structure than paddy fields). Lakes and rivers/canals are natural open-water habitats with moderate stability, assigned 5 and 4. Grassland and woodland in the study area are mostly salt-tolerant plant communities with relatively stable ecosystems, thus assigned the lowest vulnerability values of 2 and 1, respectively. Based on the above reasoning, the nine wetland types are assigned values as follows: marsh land = 9, beach land = 8, tidal flat = 7, reservoir = 6, lake = 5, river and canal = 4, paddy field = 3, grassland = 2, woodland = 1. Afterward, these values are normalized to obtain the wetland landscape vulnerability index.

Third, calculate the LER index:

$$LER_i = \sum_{i=1}^{n} \frac{A_{ij}}{A_i} \times E_i \times Q_i \quad (12)$$

Q_i is the landscape vulnerability index of wetland type i; A_{ij} is the area of wetland type i in each unit.

3. Results

3.1. Spatial and Temporal Variations in Coastal Wetland

3.1.1. Spatial and Temporal Evolution of Wetland Types

In this section, all reported areas refer to the combined total of natural and artificial wetlands unless stated otherwise. Natural wetlands include woodlands, grasslands, rivers and canals, lakes, tidal flats, beach lands, and marsh lands; artificial wetlands include paddy fields and reservoirs. The wetland areas in the YRD during different periods from 2000 to 2023 are shown in Figure 2. Over 23 years, the total wetland area initially decreased but then increased. From 2000 to 2010, it decreased by 475 km^2, followed by an increase of 867.02 km^2 over the subsequent 13 years. The dominant wetland types include reservoirs, paddy fields, marsh lands, and tidal flats. Reservoirs are primarily distributed along the northwest, northeast, and southeast coastal edges of the delta, whereas tidal flats are concentrated near the river mouth. Rivers and canals, lakes and paddy fields are found in flat areas, whereas marshes are relatively scattered and mainly surround river channels. From 2000 to 2020, the area of reservoir wetlands gradually increased, peaking in 2020. In contrast, the area of grasslands showed a continuous decline over the 23 years. The area of tidal flats expanded rapidly from 2000 to 2010 and then declined in subsequent years. The area of beach lands reached their maximum extent in 2005 and remained stable until an increase in 2020. The areas of paddy fields, woodlands, rivers and canals, and lakes exhibited minimal changes between 2000 and 2023.

To further examine wetland changes, wetland types were categorized into natural and artificial wetlands. Natural wetlands include woodlands, grasslands, rivers and canals, lakes, tidal flats, beach lands, and marsh lands, whereas artificial wetlands include paddy fields and reservoirs. The changes in natural and artificial wetlands from 2000 to 2023 are shown in Figure 3. Over this period, the area of natural wetlands steadily decreased, whereas that of artificial wetlands consistently expanded, with most of the growth occurring

after 2015. The calculations indicate that natural wetlands accounted for 76% of the total wetland area in 2000 but only 24% in 2023, with reservoirs contributing most significantly to the increase in artificial wetlands.

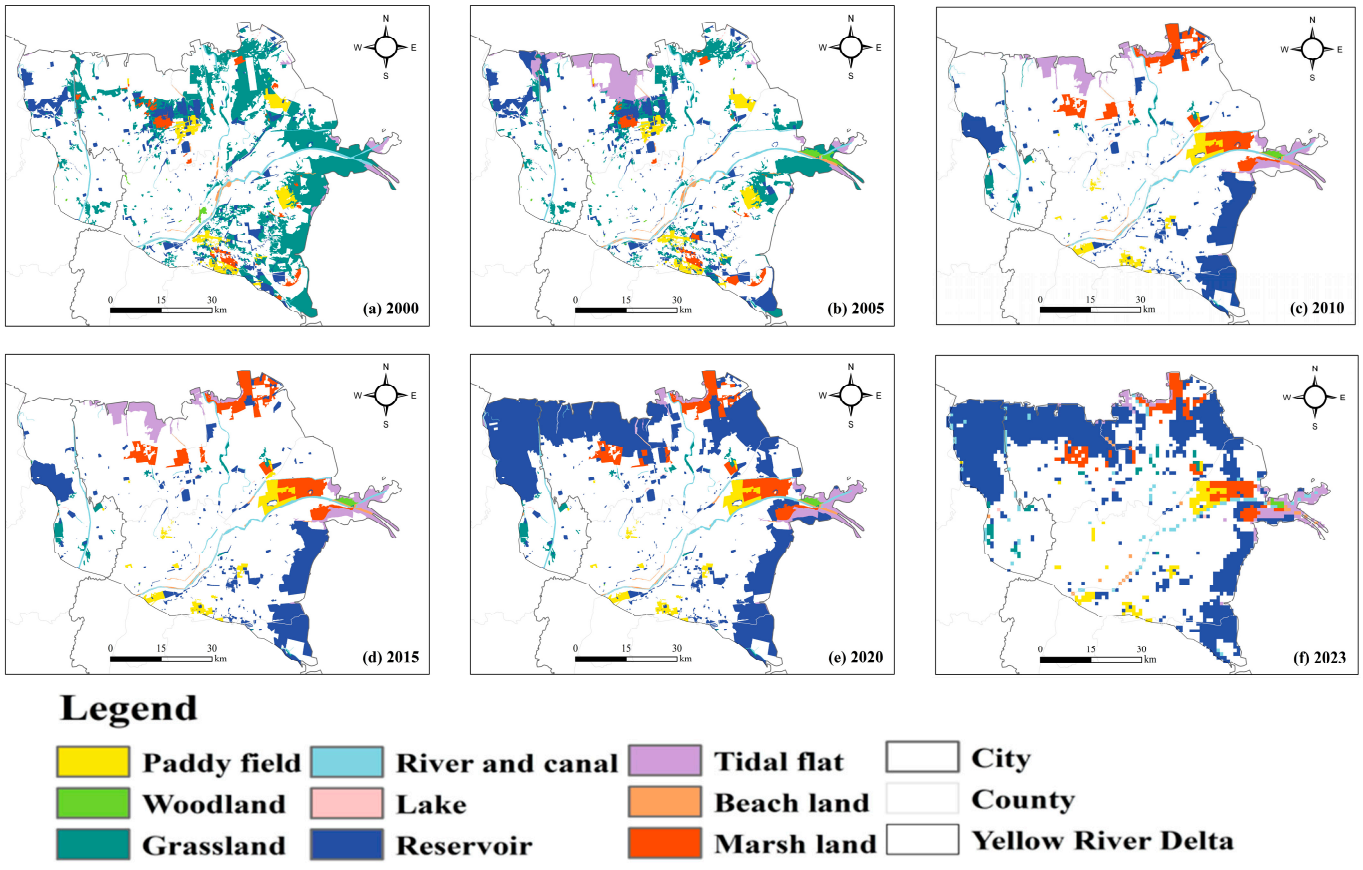


Figure 2. Spatial distribution of wetlands in the study area from 2000 to 2023 (**a**–**f**).

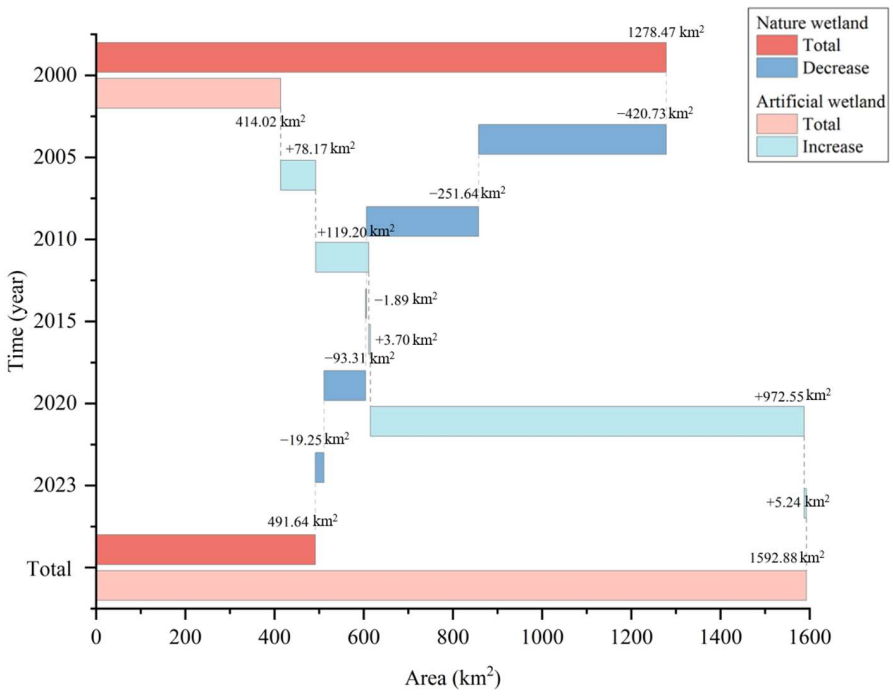


Figure 3. Changes in natural and artificial wetlands in the study area from 2000 to 2023.

The above findings reveal that wetland areas and types in the YRD changed frequently from 2000 to 2023, necessitating an analysis of wetland type transitions to understand ecological environment dynamics. The transitions between different land use types are shown in Figure 4. In this study, all land types other than the 9 wetland categories were classified as nonwetlands. Among the wetland types, grasslands and reservoirs experienced the most significant transformations during the study period. Nearly half of the grassland area was converted to nonwetlands, whereas two-thirds of the reservoir area originated from nonwetlands. The transitions between land types were frequent and complex, with land use cycling between wetland and nonwetland categories.

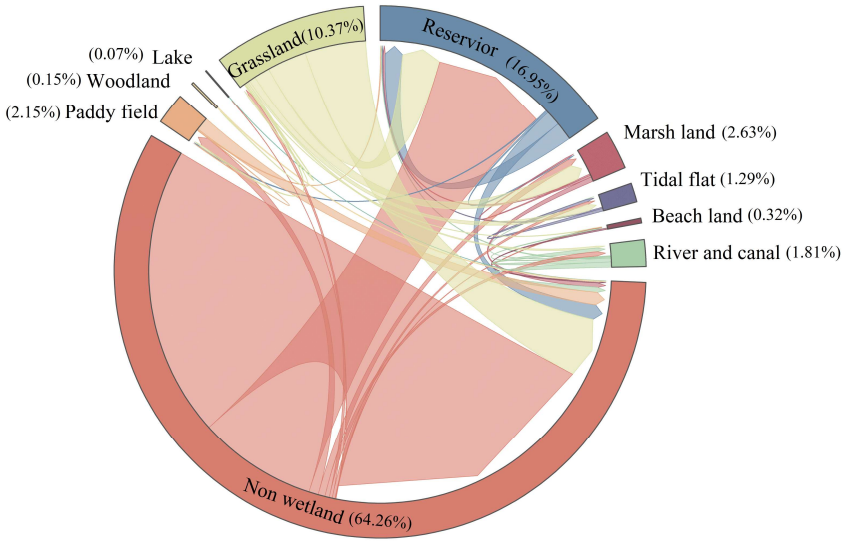


Figure 4. Transfer direction between different wetlands in study area from 2000 to 2023.

3.1.2. Migration of the Center of Gravity

This study employed the Mean Center tool within ArcGIS 10.8 to systematically investigate the spatiotemporal migration patterns of wetland centroids in the YRD, quantitatively characterizing the directional dynamics of ecological spatial configurations through centroid trajectory analysis. As shown in Figure 5, the centroid of the YRD wetlands exhibited a multi-stage trajectory between 2000 and 2023: from 2000 to 2005, it shifted 3.3 km northwest; from 2005 to 2010, it moved 1.4 km southeast; between 2010 and 2015, it remained relatively stable with a slight shift of 0.08 km southeast; during 2015–2020 and 2020–2023, it shifted 1.8 km and 0.8 km northeast, respectively. Overall, the centroid displayed a general northeastward trend, but with notable directional changes in the early and middle periods.

To further analyze the spatial distribution patterns of YRD wetlands, we conducted an SDE analysis and examined the changes in their parameters from 2000 to 2023 (Figure 6). The long axis of the SDE reflects the direction of the data distribution. In this study, the wetland distribution pattern transitioned from an east–west orientation to a northwest–southeast orientation between 2000 and 2005. By 2010, the wetland distribution returned to an east–west orientation. After 2010, the wetlands consistently exhibited an east–west distribution pattern. The short axis reflects the range of the data distribution. The length of the short axis initially increased but then decreased, with a turning point in 2010. This indicates that the wetland distribution became increasingly dispersed from 2000 to 2010, followed by gradual clustering after 2010. The ratio of the short axis to the long axis reflects the strength of directionality. From 2000 to 2015, this ratio gradually increased, indicating weakened directionality in the east–west orientation. After 2015, the ratio decreased significantly. Combined with the analysis of the long and short axes, these findings suggest that from 2000 to 2015, the directional tendency of wetlands in the east–

west orientation weakened, whereas from 2015 to 2023, the ellipse became more elongated, and the east–west directionality of wetland distribution strengthened.

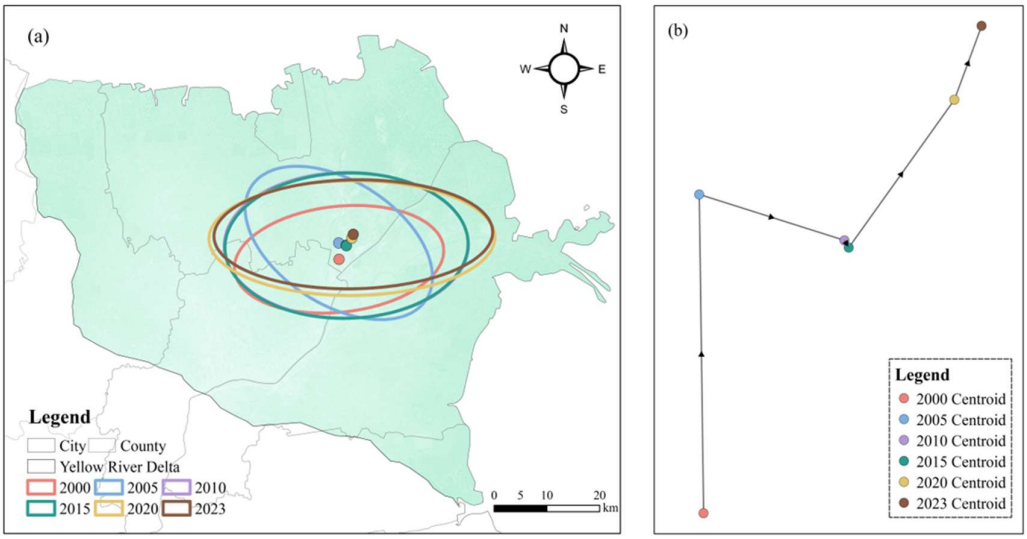


Figure 5. Migration of the gravity center of wetlands in the study area from 2000 to 2023 (**a**,**b**).

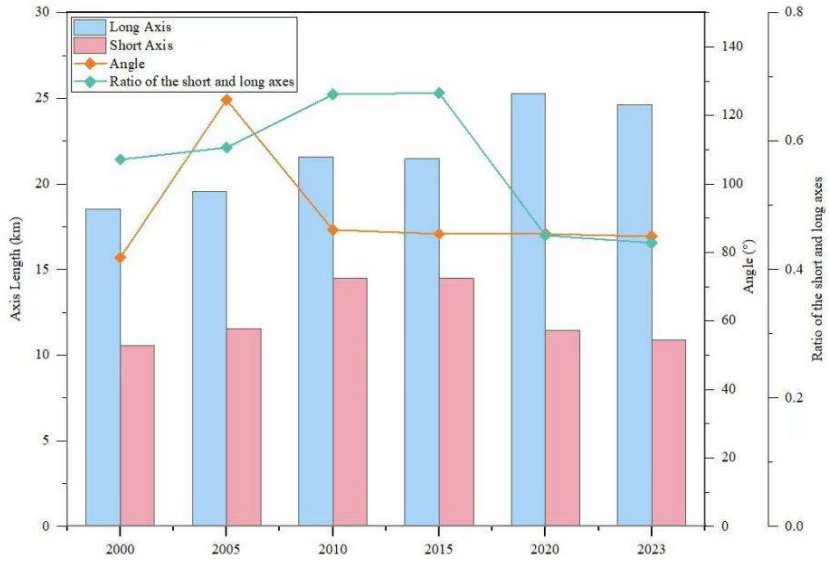


Figure 6. Variations in the standard deviation ellipse parameters from 2000 to 2023. Note: Long axis and short axis are in kilometers (km); the angle is measured in degrees clockwise from north.

3.2. Geographically Weighted Regression-Based Analysis of Wetland Drivers

After analyzing the spatio-temporal evolution of wetlands in the YRD, we selected 8 factors (precipitation (PRE), temperature (TMP), evapotranspiration (ET), fractional vegetation cover (FVC), digital elevation model (DEM), gross domestic product (GDP), population (POP), and distance to roads/railways) in both natural and human activities to study the drivers of wetland evolution using the GWR model. Before fitting, we have diagnosed the collinearity of the 8 influencing factors, and the results showed that the VIF was less than 5, and there was no collinearity among the independent variables. To ensure the applicability of the GWR model in this study, the OLS model was introduced to compare with the GWR model. The results showed (Table 1) that the AICc of the OLS model was greater than the AICc value of the GWR model in all six years, while the R^2 was smaller than the R^2 of the GWR. In 2000, the R^2 of the GWR was 0.71, but the R^2 of the OLS was only 0.12. Therefore, the GWR model was a better fit and was applicable to

this study. To further evaluate model performance, Table 2 reports the optimal adaptive bandwidth (number of nearest neighbours), the range of local R^2, and the global Moran's I of residuals for both OLS and GWR for each year. The optimal bandwidths range from 54 to 79, indicating a moderate degree of spatial non-stationarity. The local R^2 values vary across years (e.g., 0.02–0.92 in 2000), reflecting spatially heterogeneous model fit. Notably, the GWR residuals exhibit substantially lower spatial autocorrelation than the OLS residuals (e.g., 2000: OLS Moran's I = 0.58 vs. GWR Moran's I = 0.12), confirming that GWR captures most of the spatial dependence inherent in the wetland area variable.

Table 1. Comparison of fitting effect between OLS model and GWR model.

	OLS		GWR	
	AIC_c	R^2	AIC_c	R^2
2000	3121.78	0.12	2727.94	0.71
2005	3054.10	0.06	2782.39	0.61
2010	3047.63	0.13	2758.27	0.67
2015	3044.04	0.13	2689.10	0.69
2020	3069.38	0.47	2786.42	0.79
2023	3119.55	0.43	2772.31	0.79

Table 2. Summary of GWR diagnostics and residual spatial autocorrelation tests.

Year	Bandwidth (Nearest Neighbours)	Local R^2 Range	Residual Moran's I (OLS)	Residual Moran's I (GWR)
2000	54	0.02–0.92	0.58	0.12
2005	70	0.02–0.83	0.58	0.24
2010	70	0.06–0.81	0.60	0.20
2015	78	0.06–0.83	0.59	0.16
2020	78	0.25–0.95	0.48	0.17
2023	79	0.20–0.92	0.49	0.18

Table 3 presents the maximum and minimum regression coefficients for the 8 influencing factors. The missing data in Table 2 (indicated by " n.a.") arise from genuine data unavailability: ET in 2000, distance to roads/railways in 2000 and 2005, and GDP in 2023. For each year, we fitted the GWR model using only the predictors with complete data. Therefore, the predictor set varies slightly across years. To maintain meaningful temporal comparison, we focus our interpretation on the two variables that are present in all six years (TMP and POP). For other variables, we discuss only the years in which they are available and avoid direct cross-year comparisons of coefficient magnitudes. This approach, while not perfect, ensures that the reported associations are data-driven and transparent. The findings indicate that TMP is the primary natural factor influencing wetland evolution. With respect to human activities, the GDP has the most significant impact on wetland evolution, with the maximum and minimum regression coefficients in 2020 being 32.3 and −26.3, respectively. To enhance the spatial interpretability of the regression outputs, two representative determinants (TMP as a natural driver and GDP representing anthropogenic influence) were strategically selected for geospatial visualization and visualized in Figures 7 and 8.

Table 3. Maximum and minimum values of regression coefficients of 8 influential factors from 2000 to 2023.

	2000		2005		2010		2015		2020		2023	
	Min	**Max**	**Min**	**Max**	**Min**	**Max**	**Min**	**Max**	**Min**	**Max**	**Min**	**Max**
PRE	−0.205	0.603	−0.290	0.236	−0.437	0.169	−0.232	0.217	−0.176	0.115	−0.224	0.052
TMP	−28.761	36.714	−12.638	22.373	−23.778	22.757	−29.921	17.229	−8.348	10.843	−8.317	14.805
ET	n.a.	n.a.	−0.027	0.024	−0.036	0.020	−0.037	0.022	−0.025	0.013	−0.032	0.015
FVC	−0.002	0.002	−0.001	0.001	−0.001	0.001	−0.002	0.001	−0.001	0.001	−0.002	0.001
DEM	−0.660	1.615	−0.729	0.527	−0.470	0.476	−0.474	0.435	−0.598	0.495	−0.605	0.442
GDP	−21.360	31.150	−8.511	10.403	−2.603	6.487	−2.185	3.437	−26.295	32.278	n.a.	n.a.
POP	−0.311	0.281	−0.168	0.017	−0.177	0.081	−0.097	0.030	−0.022	0.040	−1.321	3.485
Distance of roads and railways	n.a.	n.a.	n.a.	n.a.	−0.001	0.001	−0.002	0.002	−0.001	0.002	−0.001	0.003

Note: "n.a." indicates that the covariate was not available for that year (see text for details). For years with missing covariates, the GWR model was fitted using only the available predictors. Consequently, direct cross-year comparisons of absolute coefficient values are performed only for variables that are present in all years (TMP and POP). All other interpretations are either year-specific or limited to years with complete data.

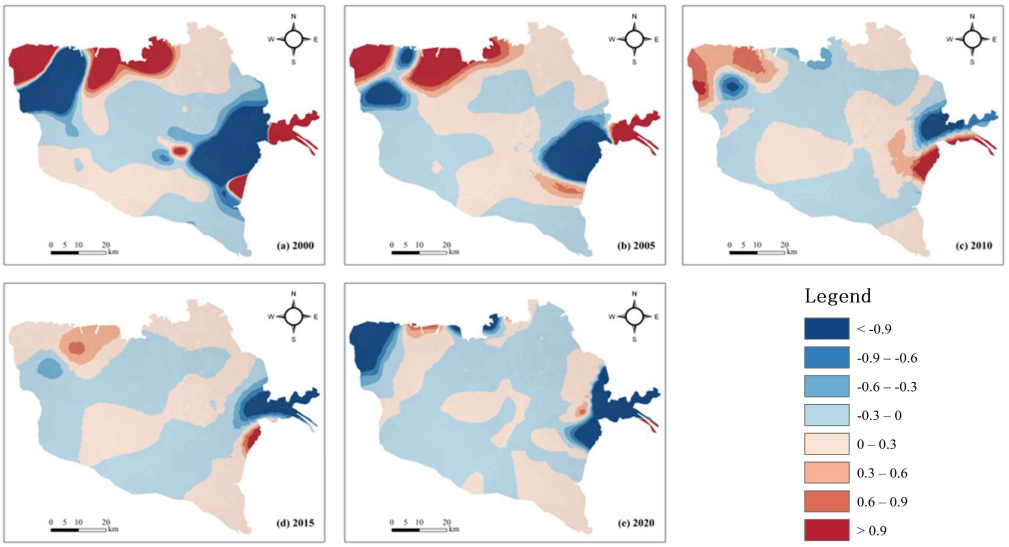


Figure 7. Regression coefficient of GDP in Yellow River Delta from 2000 to 2020.

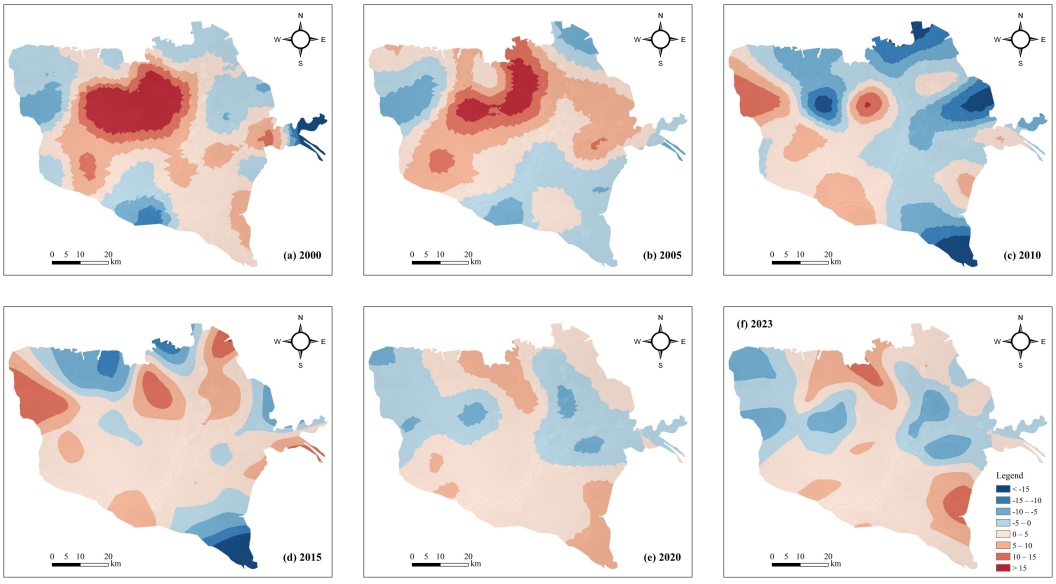


Figure 8. Regression coefficient of temperature in Yellow River Delta from 2000 to 2023.

In 2000, considering all estimated coefficients (both significant and non-significant), the GDP regression coefficients were predominantly negative in the central and southern wetlands, with negative-value regions exceeding positive-value regions overall (Figure 7). This spatial pattern suggests that in the early period, economic activities such as urban expansion and industrial development in those areas were already exerting a relatively stronger negative pressure on wetlands. By 2005, the areas with negative regression coefficients had decreased compared with those in 2000, but a region in the west emerged with statistically significant coefficients ranging from −8.5 to 3.9. The emergence of positive coefficients in the west implies that some local economic developments (e.g., aquaculture or reservoir construction) might have been positively associated with wetland area during that period. In 2010, although more than half of the regions had positive coefficients, most of these coefficients were not statistically significant, whereas the areas with statistically significant coefficients were mostly negative. This indicates that while positive associations were widespread, they were weak and likely not robust, whereas negative associations, though less extensive, were stronger and more reliable. By 2020, after a decade of development, the negative-value regions outweighed the positive-value regions, suggesting a stronger negative association between economic development and wetland status over time. The shift from a mixed to a predominantly negative association aligns with the observed acceleration of artificial wetland expansion (reservoirs and aquaculture ponds) at the expense of natural wetlands after 2010.

Similarly, TMP also shows both positive and negative associations with wetlands (Figure 8). In 2000, areas with negative coefficients were scattered along the wetland edges, whereas the central and southern wetlands predominantly presented positive coefficients. This distribution implies that temperature effects were heterogeneous: warming may have benefited wetland vegetation in the interior (e.g., by extending growing seasons) but caused water stress at the edges, where water tables are shallower and more variable. By 2005, the areas with negative coefficients were more concentrated than they were in 2000, particularly in the south, where negative-value regions corresponded to river wetlands. The concentration of negative coefficients along rivers suggests that temperature-induced evapotranspiration might have reduced water availability in riparian zones, offsetting any positive effects. In 2010, the coefficients in the northern and central-eastern regions shifted from positive to negative, resulting in more negative-value regions than positive ones. This shift could be related to a series of dry years or to land cover changes that reduced the buffering capacity of those areas against warming. However, by 2015, the number of positive-value regions once again exceeded that of negative-value regions. The return of positive associations after 2015 may be linked to increased precipitation or improved water management practices that alleviated temperature-induced water stress.

3.3. Landscape Ecological Risk Analysis

3.3.1. Characterization of Spatial and Temporal Changes in Ecological Risks

To evaluate whether and to what extent these influencing factors have threatened the wetland ecosystem, this study developed a wetland ecological risk assessment model. Using the fishnet tool in ArcGIS 10.8, the study area was divided into 665 risk evaluation units (900 m × 900 m each), and the centroid of each unit was generated. After calculating the LER index for each unit, we performed kriging interpolation to produce a continuous risk surface. To verify the robustness of the LER results to the chosen disturbance weights (0.5, 0.3, 0.2), we conducted a sensitivity analysis for the year 2020 using two alternative weighting schemes: (0.4, 0.3, 0.3) and (0.3, 0.4, 0.3). The Pearson correlation coefficients between the original and new LER values were 0.999973 and 0.999989, respectively. The global Moran's I of the original LER was 0.672, while those of the new LER surfaces were

0.673 and 0.673 (all $p < 0.001$), indicating that the spatial clustering pattern remained virtually unchanged. These results demonstrate that the LER outcomes are robust to reasonable perturbations of the disturbance weights (Table 4).

Table 4. Sensitivity analysis of disturbance weights for the year 2020.

Weighting Scheme	Pearson Correlation (vs. Original LER)	Global Moran's I
Original (0.5, 0.3, 0.2)	reference	0.672
Alternative 1 (0.4, 0.3, 0.3)	0.999973	0.673
Alternative 2 (0.3, 0.4, 0.3)	0.999989	0.673

The LER values were then classified into five risk levels—Low, Medium-Low, Medium, Medium-High, and High—using the Jenks natural breaks method. Subsequently, the areal percentage and spatial distribution of each risk class were calculated and mapped (Figures 9 and 10). The implemented framework quantitatively delineates risk stratification through zonal statistical analysis, thereby establishing a diagnostic mechanism for threat severity evaluation within coupled human-environment systems. Figure 9 shows that in 2000 and 2005, medium–low-risk areas accounted for the largest proportion of the total area. In 2010 and 2015, medium-risk areas accounted for the largest proportion, whereas in 2020 and 2023, medium–high-risk areas occupied the largest share. From a temporal perspective, between 2000 and 2005, medium–low-risk areas experienced the most significant change, decreasing by 12%, followed by an increase of 7% in medium-risk areas. Between 2005 and 2010, medium–low-risk areas again showed the largest decrease, decreasing by 16%, whereas medium–high-risk areas increased by 12%. From 2010 to 2015, the proportion of ecological risk areas remained relatively stable. From 2015 to 2020, high-risk areas exhibited the greatest increase, increasing by 13%, whereas low-risk areas decreased by 9%. Between 2020 and 2023, low-risk areas experienced the greatest increase, expanding by 8%, whereas medium-risk areas decreased by 5%. Overall, from 2000 to 2023, medium–high-risk and high-risk areas in the YRD increased significantly, whereas low-risk and medium–low-risk areas decreased significantly, indicating a trend toward increasing ecological risk values.

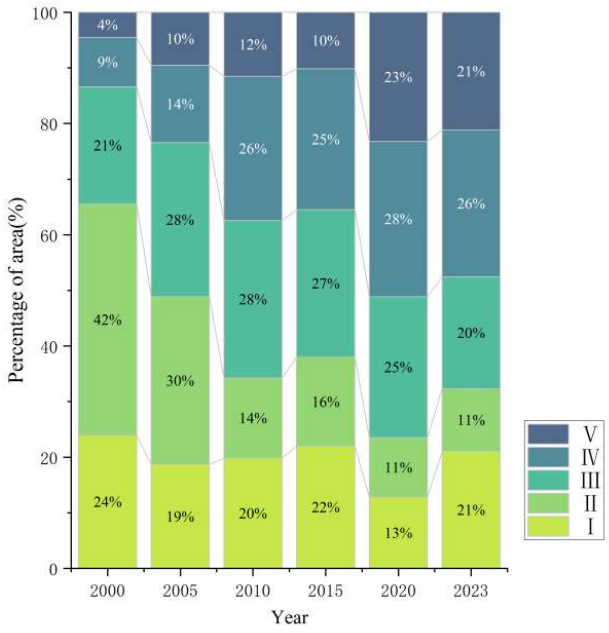


Figure 9. Changes in the percentage of low-risk, medium-low risk, medium-risk, medium-high risk and high-risk areas from 2000 to 2023.

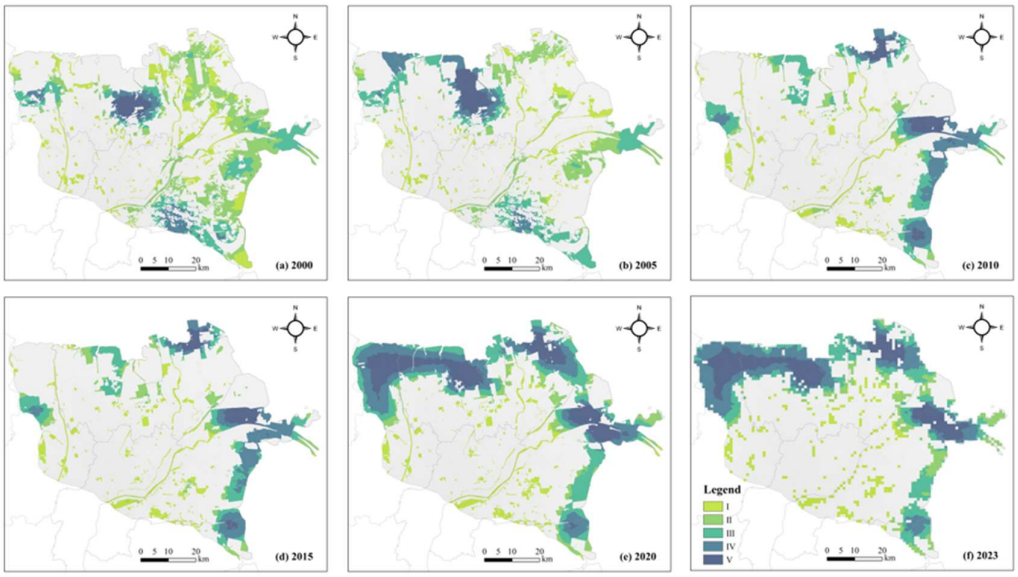


Figure 10. Landscape ecological risk of wetlands in Yellow River Delta from 2000 to 2023 (**a**–**f**). Note: In the legend, V = High, IV = Medium-High, III = Medium, II = Medium-Low, I = Low. The same color scheme applies to all panels.

To facilitate direct verification of the temporal changes described above, Table 5 presents the exact areal percentages of each LER level for all six years. Figure 10 shows that from 2000 to 2005, the spatial distribution of LER in the northwestern YRD changed significantly, with medium–high- and high-risk areas expanding. From 2005 to 2010, changes in the spatial distribution of LER were more pronounced in the southeastern delta, where low-risk and medium–low-risk areas primarily transitioned into medium–high-risk and high-risk areas and expanded. From 2010 to 2015, the overall changes in the spatial distributions of the ecological risks were minimal. From 2015 to 2020, the spatial distribution of LER in the northwestern and northern parts of the delta changed significantly, with contiguous medium–high-risk and high-risk areas emerging. Overall, the LER levels in the YRD wetlands have increased, indicating a deterioration in the LER status of the wetlands and increasingly severe ecological problems.

Table 5. Percentage of total area classified into each LER level from 2000 to 2023.

Year	Low	Medium-Low	Medium	Medium-High	High
2000	24%	42%	21%	9%	4%
2005	19%	30%	28%	14%	10%
2010	20%	14%	28%	26%	12%
2015	22%	16%	27%	25%	10%
2020	13%	11%	25%	28%	23%
2023	21%	11%	20%	26%	21%

3.3.2. Spatial Autocorrelation Analysis of Ecological Risks

Furthermore, we conducted a global Moran's I analysis to examine whether the LER level of the YRD wetlands exhibited spatial autocorrelation. Table 6 summarizes the results of the global Moran's I analysis for the LER levels of the YRD wetlands from 2000 to 2023. The Moran's I values for 2000, 2005, 2010, 2015, 2020, and 2023 were 0.49, 0.57, 0.57, 0.56, 0.67, and 0.63, respectively, all of which are greater than zero, indicating the presence of a spatial clustering pattern. The Moran's I values increased from 2000 to 2010 and from 2015 to 2020, suggesting enhanced spatial aggregation of LER, whereas the values decreased from 2010 to 2015 and from 2020 to 2023, indicating a weakening of

spatial clustering. Significance of the Moran's I was assessed using a permutation test with 999 random permutations.

Table 6. Global Moran's Index analysis results of wetland ecological risk in Yellow River Delta from 2000 to 2023.

	2000	2005	2010	2015	2020	2023
Moran's Index	0.493	0.568	0.567	0.565	0.672	0.627
Expected Index	−0.002	−0.002	−0.002	−0.002	−0.002	−0.002
z-score	21.708	24.370	22.224	22.038	28.981	24.670
p-value	$p < 0.001$	$p < 0.001$	$p < 0.001$	$p < 0.001$	$p < 0.001$	$p < 0.001$

Spatial clustering maps of the YRD wetlands for 2000, 2005, 2010, 2015, 2020, and 2023 were generated on the basis of the LER evaluation scale (Figure 11). In 2000, H–H clusters were primarily concentrated in small areas in the northern, southern, and northwestern parts of the wetlands, whereas L–L clusters were mainly located in the western region. By 2005, the area of H–H clusters in the northern region had expanded, although the locations of these clusters remained relatively unchanged. In 2010, H–H clusters were concentrated in the northeastern, eastern, and southeastern regions, whereas L–L clusters were more dispersed and were predominantly located in the central wetlands. In 2015, the clustering pattern showed minimal change compared with that in 2010. In 2020, both the H–H and L–L clusters exhibited significant increases, which also corroborates the results of the global Moran's I analysis. An H–H cluster emerged in the northwestern part of the wetlands, and the L–L cluster in the central region expanded outward. In 2023, the number of H–H and L–L clusters slightly decreased, with little change in their distribution. Overall, the majority of the YRD wetlands were characterized by H–H clusters, which spatially coincide with the medium-high and high-risk zones.

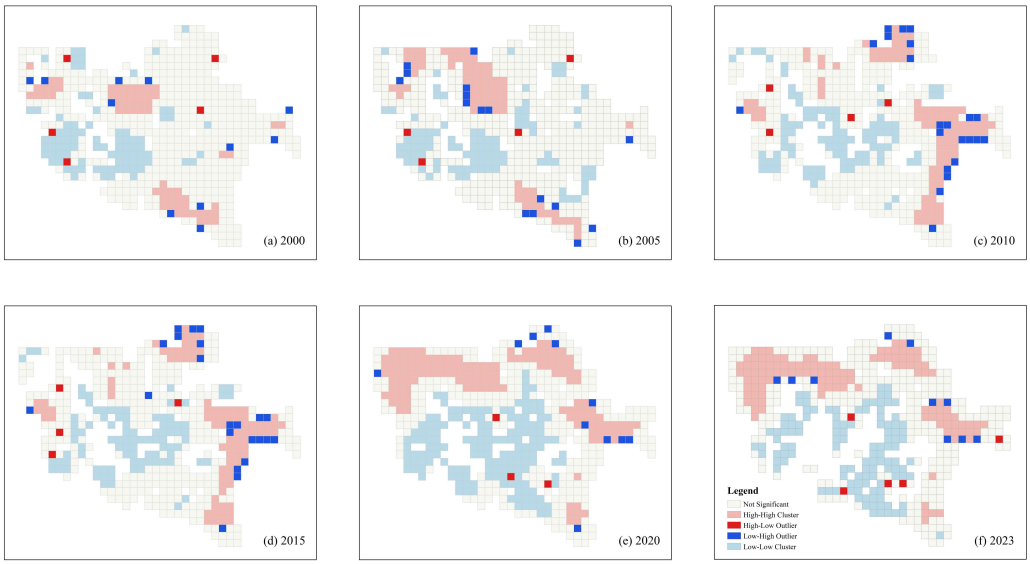


Figure 11. Spatial clustering of wetland ecological risk in Yellow River Delta from 2000 to 2023 (**a**–**f**).

4. Discussion

4.1. Explanation of the Results

The wetland area of the YRD showed a trend of initially decreasing and then increasing, which is consistent with the findings of [47]. This phenomenon is closely related to the implementation of the "National Wetland Protection Plan" and the "Wetland Protection and Management Regulations of 2013" [14]. To ensure the rational development and protection

of wetlands according to law, Shandong Province has formulated local wetland protection regulations, namely, the "Wetland Protection Measures of Shandong Province (2012)". These measures make specific provisions for the protection of wetland ecosystem integrity, the establishment of wetland nature reserves and wetland parks, and the sustainable development of wetlands, which are also related to the continuous increase in wetland area after 2010. From 2000 to 2020, the area of reservoir wetlands continued to increase, with the most significant increase occurring in 2020. This is related to the "The 13th Five-Year Plan for National Fishery Development (2016–2020)" issued by the Ministry of Agriculture and Rural Affairs of the People's Republic of China in 2016. To improve the key tasks of the "Aquaculture Water Area and Tidal Flat Planning," Shandong Province has also prepared a three-tier aquaculture water area and tidal flat plan at the provincial, municipal, and county levels.

Among the eight drivers examined, GDP and TMP showed the strongest associations with wetland evolution, with average regression coefficients that surpassed those of other factors. GDP exhibits both positive and negative associations with wetlands in the YRD, as evidenced by the spatially varying coefficients in Figure 7. This dual pattern is spatially supported by cross-referencing the GDP coefficient maps (Figure 7) with the land-use transition patterns (Figure 4). Specifically, the areas with positive GDP coefficients largely coincide with regions where non-wetlands were converted into paddy fields or reservoirs (Figure 4), reflecting the positive association through aquaculture or aquatic crop cultivation. In contrast, the areas with negative GDP coefficients correspond to regions where wetlands were converted into industrial, commercial, or other urban land (Figure 4), indicating a negative association through urban expansion. By 2020, after a decade of development, the negative-value regions outweighed the positive-value regions, suggesting a stronger negative association between economic development and wetland status over time, with the negative associations surpassing the positive ones. Similarly, TMP also shows both positive and negative associations (Figure 8); the negative associations of TMP with wetland area are likely related to increased evaporation from rising TMP, which may reduce wetland area. Beyond evaporative effects, rising temperatures have been shown to trigger additional ecological responses in the Yellow River Delta region. For instance, warming alters vegetation phenology by advancing the start of the growing season and delaying senescence, thereby modifying plant community structure and ecosystem carbon balance. Experimental warming has also been found to reduce plant water-use efficiency in seasonal hydroperiod wetlands and to impair the resistance and resilience of wetland vegetation to extreme flood events. Moreover, long-term temperature increases, combined with reduced freshwater discharge and soil salinization, have accelerated salt marsh degradation and habitat loss in the YRD. The visualization of the GWR results indicates that between 2000 and 2023, the negative associations of economic development with wetland evolution were stronger than those of natural factors such as TMP. With the intensification of human activities, natural wetlands have been increasingly converted into artificial and non-wetland areas, which may correspond to reduced wetland areas, increased fragmentation, weakened hydrological connectivity, and diminished biodiversity, among other consequences.

According to the analysis in Section 3.3.1, in terms of time, the proportion of medium–low-risk areas in the LER of the YRD gradually decreased from 2000 to 2023, whereas the proportion of medium–high- and high-risk areas increased. In 2000, medium–low-risk areas accounted for 42%, and the combined area of medium–high- and high-risk areas accounted for 13%. By 2023, medium–low-risk areas accounted for only 11%, whereas the combined area of medium–high- and high-risk areas reached 47%. Spatially, medium–high- and high-risk areas are distributed mainly on the periphery of the YRD, with their scale

gradually expanding, whereas low-risk and medium–low-risk areas are distributed mainly in the central river basins of the YRD. Overall, the LER in the YRD wetlands has shown a continuous increasing trend, which coincides with the sustained increase in artificial wetland areas, especially the expansion of reservoirs, whereas natural wetland areas have gradually decreased. The composition and structure of natural wetland ecosystems are complex, with high stability, strong ecological functions, and low ecological risk. However, artificial wetlands are a result of relatively simple human decisions, with short food chains, simple food webs, low biodiversity, weaker resistance to external disturbances, and weaker ecological functions than natural wetlands. They also face issues such as non-point source pollution and wastewater discharge. Specifically, regions dominated by reservoir and marsh land wetlands contribute to the formation of high-risk clusters, where the degree of marsh land succession is low, and they are highly influenced by environmental factors with weak resistance to disturbances. Additionally, reservoir wetlands have relatively low species richness compared with natural wetlands and exhibit simpler ecosystem structures, weaker stability, and unstable landscape structures. The findings align with Yu et al. [48], who posit that the conversion of natural wetlands to artificial wetlands constitutes a significant degradation of natural wetland ecosystems. Our analysis reveals that rapid coastal economic development has been accompanied by the extensive expansion of reservoirs (artificial wetlands), which encroach upon natural wetlands in the YRD. This spatial mismatch underscores a critical disconnect between ecological conservation priorities and regional economic growth trajectories, reflecting systemic challenges in balancing anthropogenic activities with ecosystem integrity. Therefore, on the basis of the LER situation of YRD wetlands and existing ecological protection policies, exploring sustainable economic development in the YRD while ensuring wetland ecological protection is highly practical. By reviewing the relevant literature and policies and considering the complexity and vulnerability of wetland ecosystems and the diversity of implementation entities, we propose the following recommendations for LER management in the YRD.

First, local governments should implement zone-specific land use strategies based on the spatial distribution of H-H risk clusters (Figure 11). Reservoirs, paddy fields, and other high-risk concentrated areas, which are mainly located in the northwestern and northeastern parts of the delta (where GDP coefficients were positive but H-H clusters dominate), are significant causes of ecological vulnerability. For these areas, we recommend strictly controlling new aquaculture and reservoir construction, and instead promoting ecologically healthy aquaculture models such as integrated rice-fish farming [49]. In addition, creating national-level ecological aquaculture demonstration zones in the western part of the delta (where GDP showed positive associations with wetland conversion) can help balance economic development and ecological protection. Three-dimensional ecological aquaculture systems should be established to increase biodiversity and improve ecosystem stability.

Second, ecological environment governance should be integrated with spatial risk patterns. Wastewater treatment and comprehensive environmental governance should be prioritized in the central and southern delta, where GDP coefficients were persistently negative (Figure 7) and land conversion from wetlands to urban/industrial uses was concentrated (Figure 4). Traditional fisheries production plants in those areas can be transformed into scenic, ecological, and leisure facilities (e.g., recreational fisheries, leisure fishing) only if they do not further fragment remaining natural wetlands. This approach links governance measures directly to the identified high-risk zones and negative-association areas.

Third, a risk-based management system should be established, with clear responsibilities for governments, enterprises, and individuals, specifically targeting the protection of H-H clusters and the control of artificial wetland expansion. The ecological compensation

system [14] should be refined to provide higher compensation rates for natural wetlands that are converted into high-risk artificial wetlands, thereby disincentivizing such conversions. Moreover, protected area planning should consider incorporating the H-H clusters that currently lie outside the nature reserve (Figure 11), either by extending the reserve boundaries or by creating buffer zones with restricted aquaculture activities.

4.2. Serving the Sustainable Development Goals

In recent years, global climate change and ecological issues have become increasingly prominent, and local ecological conditions should be considered in conjunction with global trends [19]. Therefore, on the basis of the data and results of this study, we assessed and analyzed the regional ecosystem in alignment with the SDGs. The SDGs, proposed to address current global issues, aim for coordinated development between the economy, society, and the environment. Among them, SDG 2, SDG 6, SDG 13, SDG 14, and SDG 15 are linked to the sustainable development of wetland ecosystems. These goals encompass ecosystems such as oceans, forests, and freshwater, reflecting the crucial role of wetland conservation in achieving the SDGs [50]. To advance the operationalization of SDGs in wetland ecosystem governance, this study strategically focuses on SDG 14 ("Life Below Water") through targeted analysis of SDG 14.2 and SDG 14.5, thereby establishing a novel evaluation framework that bridges deltaic wetland dynamics with sustainability metrics.

Guided by the specific targets of SDG 14.2—which mandates the sustainable management and protection of marine and coastal ecosystems by 2020 through enhanced disaster resilience, minimizing adverse impacts, and restoring degraded habitats to ensure ocean health and productivity—this study quantified coastal wetland area dynamics and linked them to the LER spatial patterns (Figures 10 and 11) as well as the GWR results (Figures 7 and 8) in the YRD from 2000 to 2023 [19]. The LER spatial patterns and GWR findings together highlight spatially heterogeneous risk distributions that are relevant to SDG 14.2 implementation. The spatiotemporal analysis provides a critical evaluation of policy implementation effectiveness, particularly in reconciling ecological restoration objectives with anthropogenic pressures under rapid coastal development (Figure 12). To protect the wetland ecosystems and biodiversity of the YRD, Shandong Province approved the "Regulations on the National Nature Reserve of the Shandong Yellow River Delta" in 2017 and the "Dongying Wetland Protection Regulations" in 2018. Data analysis revealed that from 2000 to 2015, the area showed a declining trend, but the decrease was small, whereas from 2015 to 2020, there was a noticeable increase in area. As discussed in the previous section, this analysis confirmed that policy management has helped restore the coastal wetland area of the YRD to some extent. However, to achieve the restoration goals outlined in SDG 14.2, the next step should consider a paradigm shift toward hybrid rehabilitation strategies, strategically integrating natural recovery processes with targeted artificial remediation techniques, to synergistically enhance ecosystem resilience while addressing the spatial heterogeneity of degradation patterns identified through GWR modeling.

SDG 14.5 stipulates, "By 2020, conserve at least 10% of coastal and marine areas, consistent with national and international law and based on the best available scientific information." To assess the response of the YRD wetland protection management policies to SDG 14.5, we used two ratios: the area of the YRD Nature Reserve to the total area of the YRD and the area of the YRD wetland reserve to the area of the YRD Nature Reserve [19]. Integrating these ratios with the LER clustering results (Figure 11), it is evident that the existing protected area network does not fully align with the spatial distribution of H–H risk clusters, implying that the mere achievement of the 10% coverage target may not automatically reduce ecological risks. In recent years, a series of legal regulations for the protection of the YRD have been introduced and revised by provincial

and municipal authorities, such as the "Dongying Yellow River Delta Ecological Protection and High-Quality Development Implementation Plan" and the "Dongying Yellow River Delta Ecological Protection and Restoration Regulations," which provide legal guarantees for ecological protection and restoration and positive responses to the SDGs. Through quantitative analysis (Figure 13), the ratios of the protected area to the total area of the YRD and the ratio of the wetland protected area to the protected area are both greater than 10%, with the latter showing a general upward trend, indicating that the YRD protection policies have met the target requirements of SDG 14.5. Nevertheless, to make SDG 14.5 more effective in practice, future spatial planning should consider incorporating the H–H risk clusters (Figure 11) and the spatially heterogeneous driver patterns (Figures 7 and 8) identified in this study.

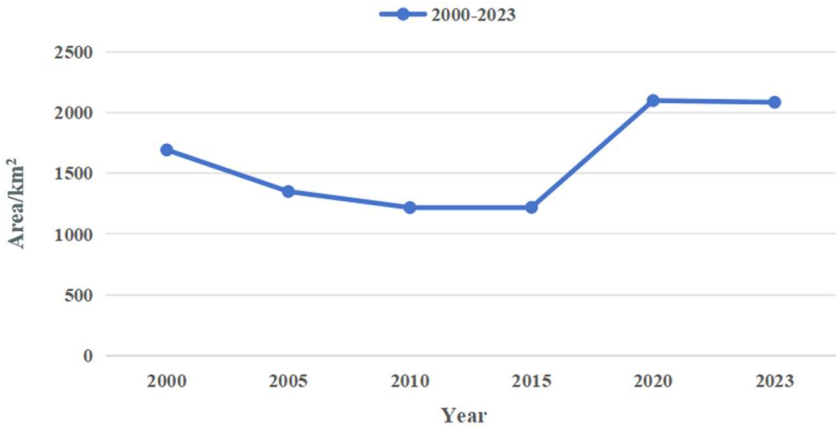


Figure 12. The area changes in coastal wetlands in the Yellow River Delta from 2000 to 2023.

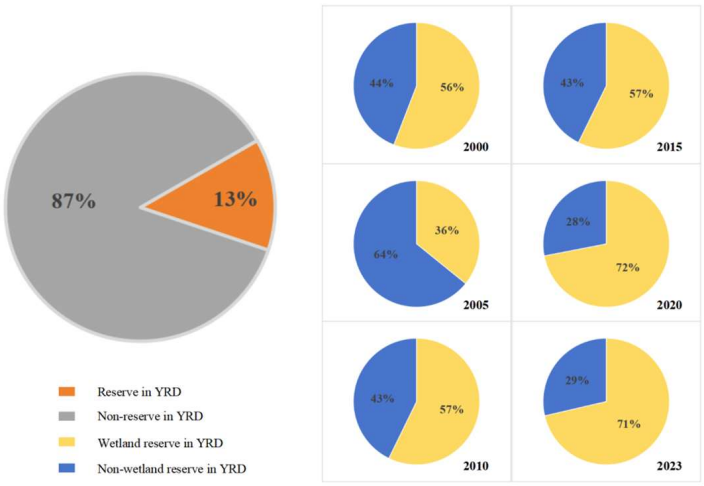


Figure 13. Protected area coverage in the Yellow River Delta (YRD) from 2000 to 2023 in the context of SDG 14.5. The two pie charts illustrate two key ratios for a representative year (e.g., 2020): (**left**) the area of the YRD Nature Reserve as a percentage of the total YRD area; (**right**) the area of wetland protected zones within the reserve as a percentage of the total reserve area.

4.3. Research Limitations

Due to challenges in data acquisition, this study selected eight available and quantifiable driving factors of wetland evolution, including meteorological, socioeconomic, topographical, and vegetation factors. However, we acknowledge that for a coastal delta system such as the Yellow River Delta, several other factors may also play important roles. These include relative sea-level rise, water salinity, sediment load and discharge from the Xiaolangdi Reservoir, ecological water replenishment volumes, and aquaculture intensity.

The absence of these variables is a limitation, as they may influence wetland dynamics—particularly the conversion of natural wetlands to artificial wetlands such as reservoirs and aquaculture ponds.

Storm surges and coastal erosion also have an impact on coastal wetlands, but owing to the challenges of spatialization, they could not be included in the GWR model. In addition, policy factors (e.g., land-use regulations, ecological restoration policies, and wetland protection plans) are recognized as critical direct drivers of wetland dynamics. However, due to their spatiotemporally lumpy nature (e.g., a policy implemented region-wide in a specific year), they cannot be easily incorporated as continuous, spatially explicit variables in the current GWR framework. We acknowledge this as a limitation.

For the analysis of driving factors in 2023, some factors used data from 2022, with a time gap of only one year; given the relatively slow rate of change in these variables, we believe this minor temporal mismatch does not substantially affect the main conclusions. Future research should attempt to integrate spatially explicit policy variables and biophysical drivers (e.g., salinity, sediment load) into ecological risk assessment to better disentangle causal pathways and improve the explanatory power of the model.

5. Conclusions

This study established a tripartite LER assessment framework encompassing "pattern evolution, driving mechanism analysis, and risk assessment" to investigate coastal wetland dynamics in the YRD from 2000 to 2023. By integrating spatial statistical methods (SDE, land use transition matrices) with the GWR model, this study systematically elucidated the spatiotemporal differentiation patterns and spatially heterogeneous associations of wetland evolution, subsequently quantifying LER. Aligned with SDG 14.2 and SDG 14.5, the analysis revealed a governance coordination lag between artificial wetland expansion and natural wetland degradation. Key findings are summarized as follows:

(1) Between 2000 and 2023, the wetland area tended to decrease, followed by an increase. Changes in land types were frequent, with land types cycling between wetland and non-wetland categories. The area of natural wetlands gradually decreased, whereas that of artificial wetlands increased, with reservoirs contributing the most to the expansion of artificial wetlands. The wetland centroid exhibited a multi-stage trajectory toward the northeast. Except for 2005, when wetlands showed a northwest–southeast distribution pattern, the wetland distribution in other years followed an east–west pattern. From 2000 to 2015, the directionality of wetland distribution weakened, whereas from 2015 to 2023, the directionality increased.

(2) From 2000 to 2023, GDP and TMP showed the strongest associations with wetland evolution, with GDP having a stronger negative association than TMP. This pattern is mainly because economic development has been accompanied by the conversion of natural wetlands into artificial wetlands, which may correspond to increased fragmentation, weakened hydrological connectivity, and decreased biodiversity, among other effects. It should be noted that GWR captures spatial associations, not causal relationships, and the incomplete set of drivers (see Section 4.3) may affect the estimated coefficients.

(3) From 2000 to 2023, the overall LER level of wetlands in the YRD showed an increasing trend, indicating that the ecological environment is under threat. In 2000 and 2005, the majority of the area was classified as low, medium-low, or medium risk. In 2010 and 2015, the areas were classified primarily as low, medium, or medium-high risk. In 2020 and 2023, the high-risk zones significantly increased compared with 2015, with the risk types being mainly medium, medium-high, and high risk. The LER exhibited

positive spatial correlation, with H–H clustering as the dominant pattern, and the H–H clustered areas coincided with the distribution of medium-high and high-risk zones.

The proposed pattern–driver–risk framework is transferable to other large deltaic systems, such as the Mekong Delta, the Mississippi River Delta, or the Pearl River Delta, where similar land–sea interactions, rapid economic development, and wetland conservation challenges exist. Future applications would need to adjust the driver selection and vulnerability scoring according to local conditions. Despite the limitations discussed in Section 4.3, the consistent methodological pipeline provides a robust basis for comparative studies across different coastal wetlands.

Author Contributions: Conceptualization, P.Z. and Y.Y.; Data curation, R.Y. and G.D.; Formal analysis, P.Z. and Y.Y.; Funding acquisition, R.Y. and X.L.; Investigation, P.Z. and L.Z.; Methodology, G.D.; Resources, X.L.; Software, Y.Y. and Z.S.; Supervision, R.Y., T.Z. and X.L.; Validation, Z.S. and M.S.; Visualization, P.Z. and T.Z.; Writing—original draft, P.Z. and Y.Y.; Writing—review and editing, X.L. All authors have read and agreed to the published version of the manuscript.

Funding: This research was supported by the Joint Research program for ecological conservation and high-quality development of the Yellow River Basin (2022-YRUC-01-0103), Watershed Non-point Source Pollution Prevention and Control Technology and Application Demonstration Project (2021YFC3201505), the National Key Research and Development Project (No. 2016YFC0502106), the Natural Science Foundation of China Research Grants (No. 41476161), and the Jing-Jin-Ji Regional Integrated Environmental Improvement-National Science and Technology Major Project (2025ZD1205000).

Institutional Review Board Statement: Not applicable.

Informed Consent Statement: Not applicable.

Data Availability Statement: The data presented in this study are available on request from the author.

Conflicts of Interest: The authors declare no conflicts of interest.

References

1. Costanza, R.; de Groot, R.; Sutton, P.; van der Ploeg, S.; Anderson, S.J.; Kubiszewski, I.; Farber, S.; Turner, R.K. Changes in the global value of ecosystem services. *Glob. Environ. Change* **2014**, *26*, 152–158. [CrossRef]
2. Ramsar Convention Secretariat. *Global Wetland Outlook: Special Edition 2021*; Ramsar Convention Secretariat: Gland, Switzerland, 2021.
3. Matovu, B.; Lee, M.-A.; Mammel, M.; Lukambagire, I.; Lutalo, B.; Mwangu, A.R.; Mwabvu, B.; Mim, T.A.; Bbira, Y.; Lubega, Y.; et al. Mobilizing evidence-based knowledge for sustainable wetlands co-management and co-governance amidst increasing anthropogenic and environmental stressors: Key lessons from Mityana District, Uganda. *Environ. Chall.* **2024**, *17*, 101014. [CrossRef]
4. Khatun, R.; Das, S. Assessment of wetland ecosystem health in Rarh Region, India through P-S-R (pressure-state-response) model. *Sci. Total Environ.* **2024**, *951*, 175700. [CrossRef]
5. Dar, S.A.; Rashid, I.; Bhat, S.U.; Dar, J.A. Evaluation of ecosystem services vis-à-vis perceptions and attitudes of local communities towards wetland conservation in Kashmir Himalaya. *Environ. Dev.* **2024**, *51*, 101041. [CrossRef]
6. Ramsar Convention Secretariat. *Global Wetland Outlook: State of the World's Wetlands and Their Services to People*; Ramsar Convention Secretariat: Gland, Switzerland, 2018.
7. Weise, K.; Höfer, R.; Franke, J.; Guelmami, A.; Simonson, W.; Muro, J.; O'Connor, B.; Strauch, A.; Flink, S.; Eberle, J.; et al. Wetland extent tools for SDG 6.6.1 reporting from the Satellite-based Wetland Observation Service (SWOS). *Remote Sens. Environ.* **2020**, *247*, 111892. [CrossRef]
8. Liu, L.; Lin, B.; Fang, Q.; Jiang, X. Effectiveness assessment of China's coastal wetland ecological restoration: A meta-analysis. *Sci. Total Environ.* **2024**, *934*, 173336. [CrossRef]
9. Sievers, M.; Brown, C.J.; Buelow, C.A.; Pearson, R.M.; Turschwell, M.P.; Adame, M.F.; Griffiths, L.; Holgate, B.; Rayner, T.S.; Tulloch, V.J.D.; et al. Global typologies of coastal wetland status to inform conservation and management. *Ecol. Indic.* **2021**, *131*, 108141. [CrossRef]
10. Peng, K.; Jiang, W.; Hou, P.; Cui, T.; Wu, Z.; Si, B. Exploring the long-term dynamics of detailed wetland types and their driving forces in coastal metropolitan areas from 1990 to 2020. *Int. J. Appl. Earth Obs. Geoinf.* **2024**, *132*, 104012. [CrossRef]

11. Kundu, S.; Kundu, B.; Rana, N.K.; Mahato, S. Wetland degradation and its impacts on livelihoods and sustainable development goals: An overview. *Sustain. Prod. Consum.* **2024**, *48*, 419–434. [CrossRef]
12. Mo, L.; Pandit, R. Wetland conservation legislations: Global processes and China's practices. *J. Plant Ecol.* **2024**, *17*, rtae018. [CrossRef]
13. Xia, S.; Xue, Z.; Dong, S.; Wu, H.; Yu, X.; Hao, Z. Identification and scoring of conservation gaps in wetlands of China's coastal provinces: Implications for extending protected areas. *J. Environ. Manag.* **2024**, *358*, 120865. [CrossRef]
14. Kang, L.; Yang, X.; Gao, X.; Zhang, J.; Zhou, J.; Hu, Y.; Chi, H. Landscape ecological risk evaluation and prediction under a wetland conservation scenario in the Sanjiang Plain based on land use/cover change. *Ecol. Indic.* **2024**, *162*, 112053. [CrossRef]
15. Li, M.; Abuduwaili, J.; Liu, W.; Feng, S.; Saparov, G.; Ma, L. Application of geographical detector and geographically weighted regression for assessing landscape ecological risk in the Irtysh River Basin, Central Asia. *Ecol. Indic.* **2024**, *158*, 111540. [CrossRef]
16. Ye, H.; Bai, D.; Wang, J.; Tan, S.; Liu, S.; Wu, X. Landscape ecological risk assessment study of the Yunnan section of the Tropic of Cancer. *Ecol. Indic.* **2024**, *158*, 111517.
17. Zeng, J.; Wu, J.; Chen, W. Coupling analysis of land use change with landscape ecological risk in China: A multi-scenario simulation perspective. *J. Clean. Prod.* **2024**, *435*, 140518. [CrossRef]
18. Che, M.; Yang, F.; Sun, J.; Zhang, C.; Zhang, J. Influence of road network expansion on the landscape ecological risk in the Yangtze River Delta region over the past two decades. *Ecol. Indic.* **2023**, *156*, 111178. [CrossRef]
19. Zhang, Z.; Jiang, W.; Peng, K.; Wu, Z.; Ling, Z.; Li, Z. Assessment of the impact of wetland changes on carbon storage in coastal urban agglomerations from 1990 to 2035 in support of SDG15.1. *Sci. Total Environ.* **2023**, *877*, 162824. [CrossRef]
20. Mo, W.; Wang, Y.; Zhang, Y.; Zhuang, D. Impacts of road network expansion on landscape ecological risk in a megacity, China: A case study of Beijing. *Sci. Total Environ.* **2017**, *574*, 1000–1011. [CrossRef]
21. Yaermaimaiti, A.; Li, X.; Ge, X.; Liu, C. Analysis of landscape pattern and ecological risk change characteristics in Bosten Lake basin based on optimal scale. *Ecol. Indic.* **2024**, *163*, 112120. [CrossRef]
22. Wang, S.; Xu, Q.; Yi, J. Multi-scale identification of driving forces for landscape ecological risk: A case study of the basin containing three plateau lakes in Yunnan, China. *Ecol. Indic.* **2025**, *170*, 113037. [CrossRef]
23. Lv, Z.; Li, S.; Xu, X.; Lei, J.; Peng, Z. Ecological risk assessment of landscape in arid area watersheds under ecological water conveyance: A case study of Taitema Lake. *Heliyon* **2024**, *10*, e29575. [CrossRef]
24. Chen, Y.; Chen, Y.P.; Xu, C.; Ye, Z. Effects of ecological water conveyance on groundwater dynamics and riparian vegetation in the lower reaches of Tarim River, China. *Hydrol. Process.* **2009**, *24*, 170–177. [CrossRef]
25. Zeng, W.; He, Z.; Bai, W.; He, L.; Chen, X.; Chen, J. Identification of ecological security patterns of alpine wetland grasslands based on landscape ecological risks: A study in Zoigê County. *Sci. Total Environ.* **2024**, *928*, 172302. [CrossRef] [PubMed]
26. Wang, Y.; Hu, X.; Wei, B.; Luo, Z.; Wang, Z.; Chen, C. Assessing landscape ecological risk in the Southern Hill and Mountain Belt of China: A 30-year analysis and future projection. *Ecol. Indic.* **2024**, *166*, 112283. [CrossRef]
27. Deng, G.; Jiang, H.; Zhu, S.; Wen, Y.; He, C.; Wang, X.; Sheng, L.; Guo, Y.; Cao, Y. Projecting the response of ecological risk to land use/land cover change in ecologically fragile regions. *Sci. Total Environ.* **2024**, *914*, 169908. [CrossRef] [PubMed]
28. Kong, X.; Kong, F.; Li, Y.; Sun, J.; Zhu, W.; Han, M. Assessment of coastal landscape fragmentation and its driving factors based on optimal scale: A case study of the Yellow River Delta, China. *Ecol. Indic.* **2024**, *166*, 112537. [CrossRef]
29. Zhang, Z.; Wang, Q.; Feng, Y.; Sun, Y.; Liu, N.; Yan, S. The spatio-temporal evolution of spatial structure and supply-demand relationships of the ecological network in the Yellow River Delta region of China. *J. Clean. Prod.* **2024**, *471*, 143388. [CrossRef]
30. Yang, Y.; Li, H.; Qian, C. Analysis of the implementation effects of ecological restoration projects based on carbon storage and eco-environmental quality: A case study of the Yellow River Delta, China. *J. Environ. Manag.* **2023**, *340*, 117929. [CrossRef]
31. Yue, X.; Sun, Q.; Lü, M.; Li, J.; Wang, A.; Zhang, S.; Xie, T.; Wang, Q. Evaluation of effects of different restoration measures on Suaeda salsa wetland in Yellow River Delta. *Environ. Eng.* **2024**, *8*, 8–16.
32. Wang, X.; Feng, A.; Hou, X.; Chao, Q.; Song, B.; Liu, Y.; Wang, Q.; Xu, H.; Zhang, Y.; Li, D.; et al. Compound extreme inundation risk of coastal wetlands caused by climate change and anthropogenic activities in the Yellow River Delta, China. *Adv. Clim. Change Res.* **2024**, *15*, 134–147. [CrossRef]
33. Guo, B.; Liu, Y.; Fan, J.; Lu, M.; Zang, W.; Liu, C.; Wang, B.; Huang, X.; Lai, J.; Wu, H. The salinization process and its response to the combined processes of climate change–human activity in the Yellow River Delta between 1984 and 2022. *Catena* **2023**, *231*, 107301. [CrossRef]
34. Sun, H.; Cui, B.; Jiang, D.; Li, Y.; Luo, Y. Dynamics and driving factors of carbon storage in the Yellow River Delta from 1980 to 2020. *Pearl River* **2024**, *45*, 36–46.
35. *GB/T 24708-2009*; Classification of Wetlands. China Standard Press: Beijing, China, 2009.
36. Chen, J.; Gao, M.; Cheng, S.; Hou, W.; Song, M.; Liu, X.; Liu, Y. Global 1 km × 1 km gridded revised real gross domestic product and electricity consumption during 1992–2019 based on calibrated nighttime light data. *Sci. Data* **2022**, *9*, 202. [CrossRef] [PubMed]
37. Zhang, Y.; Quan, J.; Kong, Y.; Wang, Q.; Zhang, Y.; Zhang, Y. Research on the fine-scale spatial-temporal evolution characteristics of carbon emissions based on nighttime light data: A case study of Xi'an city. *Ecol. Inform.* **2024**, *79*, 102454. [CrossRef]

38. Lefever, D.W. Measuring geographic concentration by means of the standard deviational ellipse. *Am. J. Sociol.* **1926**, *32*, 88–94. [CrossRef]
39. Esri. *ArcGIS Pro*, version 3.4; How Directional Distribution (Standard Deviational Ellipse) Works; Esri: Redlands, CA, USA, 2025.
40. Zhu, C.; Zhang, X.; Zhou, M.; He, S.; Gan, M.; Yang, L.; Wang, K. Impacts of urbanization and landscape pattern on habitat quality using OLS and GWR models in Hangzhou, China. *Ecol. Indic.* **2020**, *117*, 106654. [CrossRef]
41. Kashki, A.; Karami, M.; Zandi, R.; Roki, Z. Evaluation of the effect of geographical parameters on the formation of the land surface temperature by applying OLS and GWR, A case study Shiraz City, Iran. *Urban Clim.* **2021**, *37*, 100832. [CrossRef]
42. Zhang, Q.; Shen, J.; Sun, F. Spatiotemporal differentiation of coupling coordination degree between economic development and water environment and its influencing factors using GWR in China's province. *Ecol. Modell.* **2021**, *462*, 109794. [CrossRef]
43. Tobler, W.R. A computer movie simulating urban growth in the Detroit region. *Econ. Geogr.* **1970**, *46*, 234–240. [CrossRef]
44. Wang, Q.; Zhang, P.; Chang, Y.; Li, G.; Chen, Z.; Zhang, X.; Xing, G.; Lu, R.; Li, M.; Zhou, Z. Landscape pattern evolution and ecological risk assessment of the Yellow River Basin based on optimal scale. *Ecol. Indic.* **2024**, *158*, 111381. [CrossRef]
45. Du, L.; Dong, C.; Kang, X.; Qian, X.; Gu, L. Spatiotemporal evolution of land cover changes and landscape ecological risk assessment in the Yellow River Basin, 2015–2020. *J. Environ. Manag.* **2023**, *332*, 117149. [CrossRef]
46. Yin, Y.; Yang, R.; Song, Z.; Zhang, Y.; Lu, Y.; Zhang, L.; Sun, M.; Li, X. Simulation of the future evolution track of "production–living–ecological" space in a coastal city based on multimodel coupling and wetland protection scenarios. *Geogr. Sustain.* **2025**, *6*, 100237. [CrossRef]
47. Zhang, X.; Wang, G.; Xue, B.; Zhang, M.; Tan, Z. Dynamic landscapes and the driving forces in the Yellow River Delta wetland region in the past four decades. *Sci. Total Environ.* **2021**, *787*, 147644. [CrossRef] [PubMed]
48. Yu, S.; Mijiti, M.; Song, M.; Xu, J.; Yuan, D.; Xu, W. Spatio-temporal variations and influencing factors analysis of coastal wetlands in Tianjin, China. *Reg. Stud. Mar. Sci.* **2024**, *77*, 103647. [CrossRef]
49. Hua, H.H.; Cremin, E.; Huynh, D.V.; Long, G.; Renaud, F.G. Impacts of aquaculture practices on the sustainability of social-ecological systems in coastal zones of the Mekong Delta. *Ocean Coast. Manag.* **2024**, *258*, 107392. [CrossRef]
50. Jiang, W.; Wang, X.; Li, Z.; Ling, Z.; Deng, Y. Processes and future research trends of sustainable development of wetland cities. *J. Nat. Resour.* **2024**, *39*, 1241–1261. [CrossRef]

Disclaimer/Publisher's Note: The statements, opinions and data contained in all publications are solely those of the individual author(s) and contributor(s) and not of MDPI and/or the editor(s). MDPI and/or the editor(s) disclaim responsibility for any injury to people or property resulting from any ideas, methods, instructions or products referred to in the content.